ACS APPLIED MATERIALS & INTERFACES

Research Article

www.acsami.org

Effective Ligand Functionalization of Zirconium-Based Metal–Organic Frameworks for the Adsorption and Separation of Benzene and Toluene: A Multiscale Computational Study

Ying Wu,[†] Huiyong Chen,[‡] Defei Liu,[†] Jing Xiao,[†] Yu Qian,[†] and Hongxia Xi*,[†]

[†]The School of Chemistry and Chemical Engineering, South China University of Technology, Guangzhou, Guangdong 510641, People's Republic of China

[‡]School of Chemical Engineering, Northwest University, Xi'an, Shanxi 710069, People's Republic of China

Supporting Information

ABSTRACT: The adsorption and separation properties of benzene and toluene on the zirconium-based frameworks UiO-66, -67, -68, and their functional analogues UiO-Phe and UiO-Me2 were studied using grand canonical Monte Carlo simulations, density functional theory, and ideal adsorbed solution theory. Remarkable higher adsorption uptakes of benzene and toluene at low pressures on UiO-Phe and -Me2 were found compared to their parent framework UiO-67. It can be ascribed to the presence of functional groups (aromatic rings and methyl groups) that significantly intensified the adsorption, majorly by reducing the effective pore size and increasing the interaction strength with the adsorbates. At high pressures, the pore volumes and accessible surfaces of the frameworks turned out to be the dominant factors governing the adsorption. In the case of toluene/benzene separation, toluene selectivities of UiOs showed a two-stage separation behavior at the measured pressure range, resulting from the greater interaction affinities of toluene at low pressures and steric hindrance effects at high pressures. Additionally, the counterbalancing factors of enhanced π delocalization and suitable pore size of UiO-Phe gave rise to the highest toluene selectivity, suggesting the ligand functionalization strategy could reach both high adsorption capacity and separation selectivity from aromatic mixtures at low concentrations.

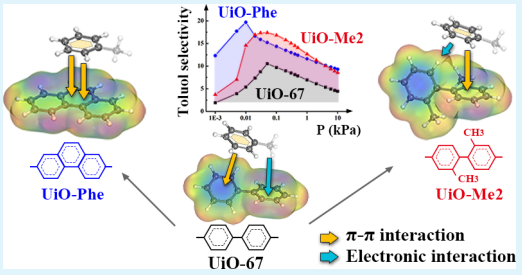

KEYWORDS: *adsorption and separation, zirconium-based metal–organic frameworks, aromatics, GCMC, DFT, IAST*

1. INTRODUCTION

Volatile organic compounds (VOCs), especially aromatic hydrocarbons such as benzene and toluene, are commonly present in emission streams from industrial activities[1] and are known to cause carcinogenicity even at extremely low concentrations.[2] Urged by the protection of environment and human health, the effective removal of VOCs has gained increasing interest worldwide.[3] The technology of adsorption, by activated carbon,[4] zeolites,[5] and other conventional porous materials, has shown great promise to alleviate VOCs emission due to its advantages of ease operation, low energy consumption, and small need for finance investment.[6] However, the application of activated carbons are hindered by their structural irregularity and flammability,[7] while zeolites show shortcoming of low interaction affinity with organic components.[8]

Metal–organic frameworks (MOFs) have been considered as one of the most promising alternatives, owing to their dense aromatic linkers and highly ordered and tunable structures[9] for high adsorption/separation performance of various organic molecules.[10,11] However, the practical applications of MOFs were limited by their low stability upon exposure toward water vapor.[12,13] As a new family of porous MOFs, the zirconium-based UiO frameworks[14] have aroused enormous attention. Integrating the merits of highly charged oxophilic Zr(IV) cations as well as the high nuclearity of Zr-based SBU, UiO-66 possesses remarkable thermal, chemical, and mechanical stabilities,[15] which made them potential robust adsorbents for various applications, such as hydrogen storage,[16] CO_2 capture,[17] etc. With respect to the adsorption and separation of aromatic VOCs, UiO-66 exhibits higher selectivity to benzene over *n*-hexane, which could be attributed to the $\pi-\pi$ stacking interaction between benzene and the MOF linkers.[18] The material can also be extended to synthesize macroporous composites, aiming to improve the transport properties of benzene and *n*-hexane.[19] Additionally, Chang et al.[20] reported the high adsorption selectivity of UiO-66 for benzene homologues from structural isomers, owing to the reverse shape selectivity and the molecular sieving effect of the framework. On the other hand, it should be mentioned that the variation of connectivity and symmetry of Zr cluster can provide different pore shape and chemical stabilities of Zr-MOFs.[21] DeCoste et al.[22] indicated that both chemical and thermal stability of Zr-MOFs would decrease gradually by

Received: December 4, 2014
Accepted: February 20, 2015
Published: February 20, 2015

DOI: 10.1021/am508570d
ACS Appl. Mater. Interfaces 2015, 7, 5775–5787

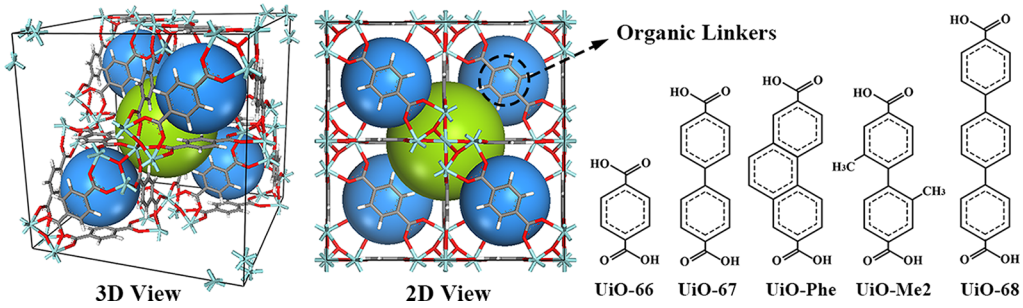

Figure 1. Schematic of three- and two-dimensional (3D and 2D) views of unit cells and the organic linkers of UiOs. The green and blue spheres represent the void regions inside the octahedral and tetrahedral cages, respectively. Color code: Zr = cyan; C = gray; O = red; H = white.

increasing the length of organic linkers. Fortunately, the small, hard Zr^{4+} ions with high charge density can still bond more strongly to carboxylates than larger, soft ions like Zn^{2+}.[23] Although UiO-67 showed decreased chemical stability compared to UiO-66, UiO-67 can still maintain structural stability when exposed to various organic solvents (e.g., pyridine, acetone, methanol, etc.), and it possesses comparative thermal stability as UiO-66 does.[22] However, to the best of our knowledge, very limited study has been carried out on the adsorption and separation of aromatic VOCs at low concentrations. As aromatics generally are present in very dilute streams in most industrial applications,[24] it is highly desired to tune the MOF structures for efficient removal of aromatic VOCs at low concentrations.

On the basis of the target, many recent experimental studies have been focused on the functionality of UiO materials. Duerinck et al.[25] reported that decorating the ligands of UiO-66 with methyl groups had positive contribution to the stereo-selective separation of aromatic homologues at low pressures, but the polar functional group ($-NO_2$) showed less influences. The hybrid materials combined UiO-66-NH_2 with microporous organic networks (MON) showed excellent performance of selective adsorption of toluene in water.[26] The postsynthetic exchange of ~50% Zr by Ti in UiO-66 is capable of dramatically enhancing CO_2 uptakes[27] due to the reduction of framework density, which may also have promising performance for aromatic adsorption. The previous works enhanced aromatic adsorption majorly by decreasing the pore size or density of the framework; however, other strategies such as the intensification of the $\pi-\pi$ stacking interaction are still lacking, which can be complemented by computational techniques. Since the synthesis of functionalized materials is usually expensive and time-consuming, the simulation approach may provide useful insights of adsorption mechanism to the atomic level and clarify the structure−property relationship of functionalized MOFs for aromatics adsorption, which may be difficult to tackle by experimental methods. Additionally, as one of the most common pollutants in industrial processes, benzene and toluene are worthy to be examined using the adsorption approach with UiO-series adsorbents, which, however, was studied in very limited literatures.[24,28]

In this work, we theoretically fabricated two new UiO structures, namely, UiO-Phe and UiO-Me2, by ligand functionalization based on UiO-67. Multiscale simulations were undertaken to obtain the fundamental understanding of adsorption and separation properties of benzene and toluene over the fully dehydrated UiO-66, -67, -68 and the two functionalized analogues. The single-component adsorption isotherms of the two aromatics over the frameworks were calculated by grand canonical Monte Carlo (GCMC) simulation, from which the density distribution contours were also gained to study the adsorption sites on the frameworks. Density functional theory (DFT) calculations were subsequently employed to obtain the energy-minimum adsorption configurations and the corresponding binding energies of benzene and toluene. Furthermore, the adsorptive selectivities of toluene/benzene mixtures are predicted by ideal adsorbed solution theory (IAST) approach. The objective of this work is to investigate the effects of functional groups (aromatic rings and methyl groups) and explore the structure−property relationship, which may provide valuable guidance for constructing new MOFs with high performance for aromatic adsorption and separation.

2. MODEL AND COMPUTATIONAL DETAILS

2.1. Model Constructions. The structural models of UiO-66, -67, and -68 were constructed on the basis of the experimental X-ray diffraction (XRD) data obtained from the Cambridge Crystallographic Data Centre.[14] The dehydrated Zr-MOF structures were subsequently constructed by removing 2 equiv of water in each $Zr_6O_4(OH)_4$ cluster, leading to the formation of inner Zr_6O_6 cluster with significant Zr Lewis acid sites.[18,29] The unit cell of the UiOs contains one large octahedral cage, surrounded by eight small tetrahedral cages that interconnected with the former through triangular windows, as illustrated in Figure 1. Since Cavka et al.[14] have claimed that the structural topology of UiOs will not alter by changing the organic linkers, we could reasonably functionalize the ligands of dehydrated UiO-67 with additional aromatic rings and methyl groups to fabricate two new-type UiOs (UiO-Phe and UiO-Me2). We determined the locations of the functional groups by means of geometry optimization using Forcite module in Material Studio Version 5.0.[30] The framework atoms were treated as relaxed and described by the universal force field (UFF). The optimization process involved energy minimization and unit cell dimensions by means of smart algorithm, with the parameter sets as 1×10^{-5} kcal mol^{-1} (energy), 0.0005 kcal mol^{-1} $Å^{-1}$ (forces), and 5.0×10^{-6} Å (displacement), respectively.

2.2. Interatomic Potentials. For the adsorption simulations, both electrostatic and van der Waals (VDW) interactions were required to guarantee the accuracy of the calculation. The long-range electrostatic interactions were treated by the Ewald summation technique, while the VDW interactions was described by 12−6 Lennard-Jones (LJ).[31] The benzene molecule was treated as a nine-site united atom model with the LJ parameters taken from the TraPPE-UA force fields.[32] The pseudo united-atom of aromatic CH group

DOI: 10.1021/am508570d
ACS Appl. Mater. Interfaces 2015, 7, 5775−5787

contained no partial charge (q_{CH} = 0 e), while three extra electrostatic sites (site 1 = +2.42 e, site 2 = −1.21 e) were employed to describe the quadrupole moment of benzene.[33] In the case of toluene, the treatment of aromatic CH groups was identical to benzene, while the CH_3 group was defined as a single interaction site using the TraPPE-UA force fields.[34] Because of the addition of methyl group, the central positive charge (site 1) of toluene turned out to be slightly closer to methyl group, similar to the anisotropic united atom (AUA) model.[35] The details of aromatic models as well as the LJ parameters and partial charges were shown in Supporting Information, Figure S1 and Table S1.

In terms of UiO frameworks, Duerinck et al.[25] have elucidated that both UFF and Dreiding force fields could provide results that are close to those of the experimental data of aromatics adsorption, whereas UFF demanded less computational resources at the similar error margins. We therefore chose UFF force field to describe the VDW interactions between adsorbates and frameworks with rationality, which has been successfully employed with other MOFs.[1,8,36,37] In addition, the partial charges for the framework atoms were obtained from previous works,[38,39] which were estimated by means of DFT calculations using Gaussian 09 package.[40] By using the unrestricted B3LYP functional with adoption of ChelpG method, the LANL2DZ basis set was used for Zr atoms, while 6-31+G* was used for the rest of the atoms. The charge distribution approach has been validated by the good correspondence between adsorption isotherms and mechanisms in MOFs.[38,39,41] The atomic charges assigned to the MOF linkers were capable of describing the conjugated π system above both sides of the linkers, which have been widely employed to study the $\pi-\pi$ interactions between aromatic molecules and MOF linkers.[9,18,42] The LJ parameters and the distribution of partial charges of UiO frameworks were listed in Supporting Information, Table S1.

2.3. Simulation Methodology. GCMC simulations were employed to investigate the adsorption isotherms and the density distribution of single components benzene and toluene in UiOs by using MUISC code.[43] The fugacity used in the GCMC calculations was converted from the corresponding pressure by means of Peng−Robinson (PR-EOS) equation of state.[44] The simulation box consisted of 2 × 2 × 2 unit cells, and the periodic boundary conditions (PBC) were applied in all three dimensions. With a spherical cutoff radius of 13.0 Å applied for LJ interactions, all the framework atoms were treated as frozen at their crystallographic positions, similar to previous works on UiOs.[18,38,45,46] During GCMC calculations, four types of trials involving translation, insertion, deletion, and rotation were randomly applied for the adsorbate molecules. For each state point of simulations, the first 5×10^6 steps were used for equilibration, followed by another 5×10^6 steps for the calculation of ensemble averages.

To compare with experimental data, the simulated (absolute) adsorption amounts (N_{abs}) should be converted to the excess adsorption amounts (N_{ex}) using eq 1.[47]

$$N_{ex} = N_{abs} - V_g \rho_g \tag{1}$$

Where ρ_g is the density of bulk gas, and V_g represents the free-guest pore volume within adsorbent for adsorption and can be estimate using helium as nonadsorbing probes, as reported by Talu and Myers.[48] Additionally, the accessible surface areas (S_{acc}) of the frameworks were calculated using nitrogen molecules as probes in a Monte Carlo program proposed by Düren and Snurr.[47] The calculated S_{acc} and V_g values are listed in Table 1.

Table 1. Textural Properties of UiOs and MOFs Studied in This Work

MOFs	cell angle (deg)	lattice (Å)	S_{acc} (m^2/g)	V_g (cm^3/g)
UiO-66[a]	$\alpha = \beta = \gamma = 90$	$a = b = c = 20.98$	1082.63	0.44
Cu-BTC[b]	$\alpha = \beta = \gamma = 90$	$a = b = c = 26.34$	2006.26	0.81
UiO-67[a]	$\alpha = \beta = \gamma = 90$	$a = b = c = 27.09$	3179.27	1.11
IRMOF-1[b]	$\alpha = \beta = \gamma = 90$	$a = b = c = 25.83$	3519.78	1.34
UiO-68[a]	$\alpha = \beta = \gamma = 90$	$a = b = c = 33.33$	4338.07	1.81
MIL-101[b]	$\alpha = \beta = \gamma = 90$	$a = b = c = 88.20$	3211.35	1.74
UiO-Me2[a]	$\alpha = \beta = \gamma = 90$	$a = b = c = 26.04$	1808.69	0.78
UiO-Phe[a]	$\alpha = \beta = \gamma = 90$	$a = b = c = 26.09$	2393.89	0.91

[a]Calculated in this work. [b]Taken from the data in the literatures.[68−70]

To clarify the thermodynamic interactions between adsorbate and adsorbent in the ideal dilute gas phase, the isosteric heats of adsorption were calculated by eq 2.[49]

$$q_{st} = RT - \left(\frac{\partial\langle v\rangle}{\partial\langle N\rangle}\right)_T \tag{2}$$

where $\langle v\rangle$ is the average potential energy of the adsorbed phase, $\langle N\rangle$ is the average number of molecules adsorbed, T is the temperature (K), and R is the ideal gas constant.

For binary mixtures, the adsorptive selectivities were computed by eq 3.

$$S = \frac{x_1}{x_2} \times \frac{y_2}{y_1} \tag{3}$$

Where x_i and y_i represent the mole fraction of component i (i = 1 or 2) in the adsorbed and bulk phases, respectively. Previous works[50,51] have shown that the value of selectivity could be estimated by both GCMC simulations and the IAST. However, GCMC calculations demand more computational resources due to the variations of shapes and interaction types of different adsorbates, and the statistical uncertainty of GCMC algorithm may lead to underestimated data of selectivity, while IAST results were more computationally stable due to its thermodynamic consistency,[50] which has been clarified to be one of the most promising procedures to indicate the separation behaviors in MOFs.[52,53] Hereby, we believed that IAST is a more reliable approach to predict the separation properties in this work. During IAST calculations, it was crucial to select a model that can precisely fit the adsorption data at the measured pressure range. We have tested several models and found the dual-site Langmuir−Freundlich (DSLF)[54,55] to be the most satisfactory model for the isotherms on the UiOs, as shown in eq 4.

$$N = N_1 \times \frac{b_1 p^{(1/n_1)}}{1 + b_1 p^{(1/n_1)}} + N_2 \times \frac{b_2 p^{(1/n_2)}}{1 + b_2 p^{(1/n_2)}} \tag{4}$$

where N is the adsorbed amount per mass of adsorbent (mmol/g), N_1 and N_2 are the saturation capacities of sites one and two per mass of adsorbent (mmol/g), p is the total bulk pressure (kPa), and b and n are the affinity coefficients and the deviations from the ideal homogeneous surface, respectively. The fitting parameters were listed in Supporting Information, Table S2. The correlation coefficients (R^2) of all the fitting

DOI: 10.1021/am508570d
ACS Appl. Mater. Interfaces 2015, 7, 5775−5787

isotherms were over 0.99, indicating the models could compute the integration of IAST with acceptable accuracy.

The energy-minimum configurations and the corresponding binding energies (BEs) between adsorbates and frameworks were obtained by DFT approach using Gaussian 09.[40] Since the adsorption of benzene and toluene at low pressures majorly occurred near the organic linkers (which were clarified in Section 3.2), where the dispersive interactions play dominant role,[18,25] we performed static DFT calculations with ωB97X-D functional[56] to qualitatively study the interactions. ωB97X-D is a long-range hybrid density functional that complemented with empirical atom−atom dispersion corrections, which has been justified to offer superior performance for the $\pi-\pi$ interactions.[57] Similar to previous works,[58,59] the cluster models of organic linkers were used for the DFT calculations, with the dangling bonds terminated by H atoms to maintain the correct hybridization. The adsorbate molecules were left relaxed, and the organic linkers were held fixed to replicate bulk behavior. In the common practices, running the geometry optimizations at low-level theory prior to the single-point energy calculations at higher level is as effective as performing all the calculations at high level.[60] Therefore, the geometry optimizations at a low level of ωB97X-D/6-31G(d, p) was used to find the energy-minimum configurations, while a higher level of ωB97X-D/6-311++G(d, p) was employed for the single-point energy calculations, similar to the DFT calculations for benzene over zeolites.[60] In BE calculations, the counterpoise correction[61] applied to the optimized structures was taken into account for basis set superposition error (BSSE).

The value of BE was calculated by subtracting the sum of the single-point energies of adsorbate ($E_{adsorbate}$) and the ligand cluster (E_{ligand}) from the energy of the optimized adsorbate-cluster complex ($E_{ligand\text{-}adsorbate}$), as shown in eq 5. A more negative BE value indicates a stronger adsorption.[62] For each molecular complex, a variety of possible configurations were tested, but only the ones with energy minimum were discussed in detail.

$$BE = E_{ligand-adsorbate} - (E_{ligand} + E_{adsorbate}) \quad (5)$$

3. RESULTS AND DISCUSSION

3.1. Effects of the Interatomic Interactions. To validate the LJ-based force field and partial charges applied in this work, the simulated excess adsorption isotherms of benzene over dehydrated UiO-66 with and without electrostatic interactions (EI) at 313 K were compared to the referred experimental data from Ramsahye's work,[18] as shown in Figure 2. Both simulated models showed a good consistency with the experimental results at the pressures below 1 kPa, whereas the model with EI exhibited slightly underestimated data at higher pressures. The explanation of the discrepancy could be associated with the capillary condensation. The well-defined opening pores of UiO-66 with diameter of 6 Å[14] were obviously ranged in the micropores,[63] offering environment for the capillary condensation. Zhao et al.[33] claimed that the benzene molecule modeled without EI (six-site model) was prone to liquefy much more easily than the nine-site model at a given pressure. The two complementary effects corporately resulted in the underestimation of nine-site model at high pressures, coincided with the adsorption behavior of benzene over IRMOF-1.[8] However, such shortcoming of the nine-site model did not affect its accuracy when modeling the adsorption at low

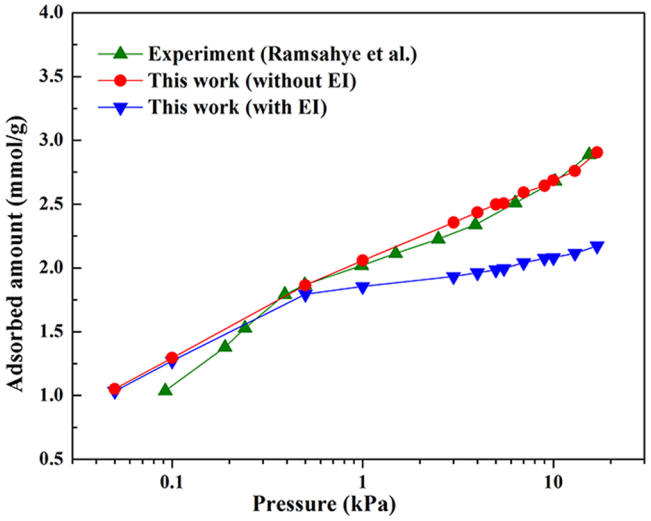

Figure 2. Simulated adsorption isotherms of benzene on UiO-66 with and without electrostatic interactions (EI) at 313 K in this work, and the referred experimental data reported by Ramsahye et al.[18]

concentrations with both dispersive and electrostatic interactions, as concerned in this work. Thus, the nine-site model was selected for modeling the adsorption over UiO-66.

In the case of UiO-67 and UiO-68, since there were no experimental data available for aromatic adsorption, we calculated the H_2 adsorption isotherms and compared the results with the referred experimental results from Chavan et al.[64] and the theoretical results from Getman et al.,[65] as shown in Supporting Information, Figure S3. These simulated isotherms showed a generally good agreement with the corresponding data from literature, validating the accuracy of force field as well as the atomic charges for the frameworks. In addition, the role of electrostatic interactions on aromatic adsorption over UiO-67 and -68 were also examined, as shown in Figure 3. In contrast to UiO-66, both models with and without EI in the interatomic interactions exhibited similar adsorption behaviors on UiO-67 and -68. UiO-Phe and UiO-Me2 also showed the similar adsorption behaviors, as illustrated in Supporting Information, Figure S4. The isotherms of toluene climbed quickly at low pressures, whereas the adsorption capacity of benzene exceeded that of toluene as the pressures rose. It was possibly because the presence of methyl group in toluene induced the stronger interaction with the frameworks at low pressures, while the steric hindrance caused by the bulky size of toluene gave rise to lower adsorption uptakes at higher pressures. On the other hand, the obtained results indicated negligible effects of EI on the adsorption isotherms of aromatics, unlike the significant role of EI in VOCs adsorption on Cu-benzene tricarboxylic acid (Cu-BTC).[66] It could be associated with the larger pore size of UiO-67 (8 Å) and -68 (10 Å),[14] which diminished the effects of capillary condensation and the variation of adsorption on these two electrically contrastive models. However, because of the significant role of extra electrostatic sites to represent the conjugated π system in benzene and toluene molecules (as mentioned in Section 2.2), we believed that the nine-site models of adsorbates containing electrostatic interactions were more accurate to proceed with the following studies in the adsorption on UiOs, including the functionalized UiO-Phe and -Me2.

Figure 4 showed the adsorption isotherms of benzene on dehydrated UiO-66, -67, and -68 at 313 K. The adsorption

DOI: 10.1021/am508570d
ACS Appl. Mater. Interfaces 2015, 7, 5775−5787

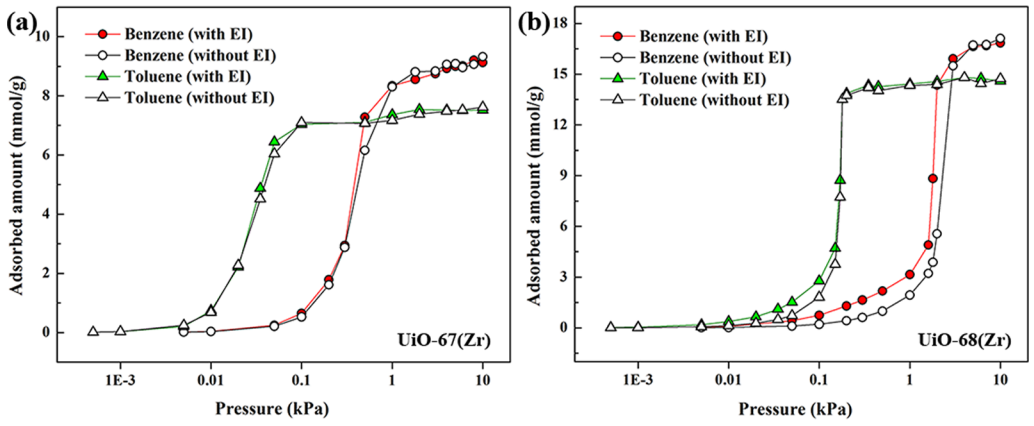

Figure 3. Simulated adsorption isotherms of benzene and toluene on (a) UiO-67 and (b) UiO-68 calculated with and without EI at 330 K.

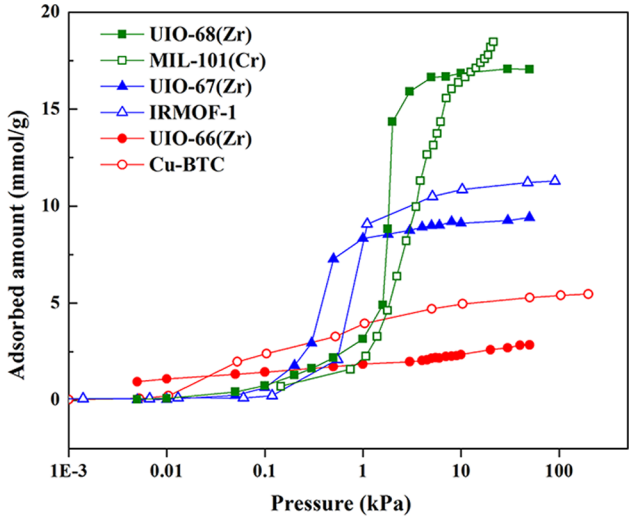

Figure 4. Simulated adsorption isotherms of benzene on dehydrated UiOs in this work and the correlation data of MIL-101, IRMOF-1, and Cu-BTC in the literature.[8,67]

uptakes on UiOs at low pressures (below 0.5 kPa) increased with decreased S_{acc} and V_g values (Table 1), following the order of UiO-66 > UiO-67 > UiO-68, while the opposite order of adsorption uptakes was observed at higher pressure range (over 5 kPa). UiO-66 possessed highest capacity at low pressures as its smallest S_{acc} (1082.63 m^2/g) and V_g (0.44 cm^3/g) offered the strongest adsorption affinity to benzene, which was in a good agreement with the preferential adsorption of CO_2 in the small pores of ZIF-94 and ZIF-7.[71] However, such structural properties of UiO-66 also dramatically hindered the adsorption at higher pressures due to the steric effects. Therefore, UiO-66 has a relatively continuous adsorption behavior in the measured pressure range. By contrast, the relatively large pores of UiO-67 and -68 caused weaker adsorption affinity at low pressures but were capable of accommodating more adsorbate molecules at adsorption equilibrium. Besides, the wider gap of pore size between tetrahedral and octahedral cages of UiO-67 and -68 may lead to the sequential adsorption, resulting in the two-stage adsorption isotherms.

On the other hand, the adsorption isotherms of the dehydrated UiOs were also compared with other MOFs with varied open metal sites, including Cu-BTC, IRMOF-1, and MIL-101,[8,67] as shown in Figure 4. It was interesting to find that the isotherms of UiOs were similar in shape compared to the MOFs with analogous pore volumes (UiO-66 and Cu-BTC, UiO-67 and IRMOF-1, UiO-68 and MIL-101, respectively). The result reveals that not only the open metal sites provide significant interaction affinity with adsorbates, but the textural properties (majorly determined by organic linkers) also play roles in the adsorption, consistent with the size-dependency of aromatic adsorption over UiOs reported by Duerinck et al.[25] Therefore, to improve the adsorption of aromatics, the functionalization strategy would be recommended to focus on

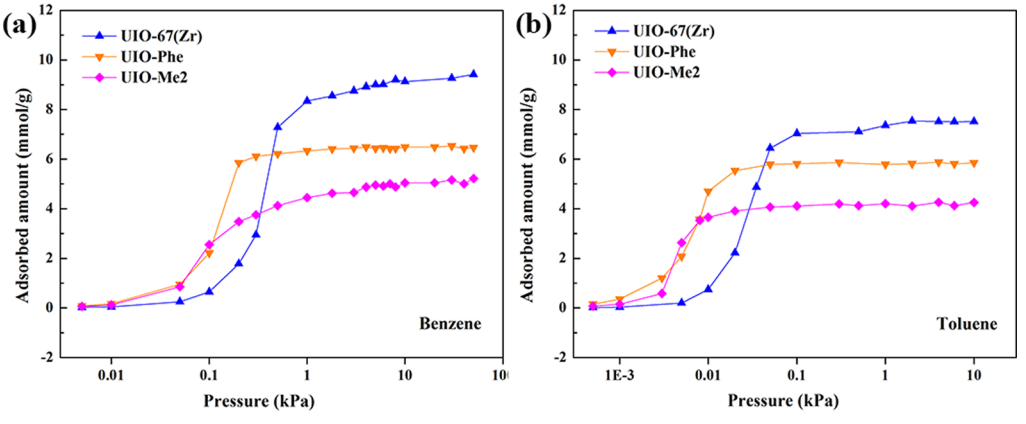

Figure 5. Simulated adsorption isotherms of (a) benzene and (b) toluene on UiO-67, -Phe, and -Me2 as a function of pressures at 330 K.

DOI: 10.1021/am508570d
ACS Appl. Mater. Interfaces 2015, 7, 5775−5787

the organic linkers, by enhancing the interaction strength or changing the pore size.

3.2. The Adsorption on Functionalized Frameworks. When introducing UiO-67 with functional groups, the effects of functionalization on the structure of the framework were required to be clarified prior to further investigating the adsorption properties. It could be noted in Table 1 that UiO-Phe (26.09 Å) and UiO-Me2 (26.04 Å) possessed lower lattice length compared to the original UiO-67 (27.09 Å), indicating that the unit cells of the frameworks were slightly compressed due to the addition of functional groups. In addition, as shown in Supporting Information, Figure S5, compared to UiO-67 (40.3°), the optimized linker in UiO-Phe transformed to planar (180°), while the two phenyl rings in UiO-Me2 turned to be almost perpendicular (82.9°) to each other. Such conformation of linkers in UiO-Phe allowed the framework suffer less steric hindrance effects and gave rise to larger S_{acc} and V_g than UiO-Me2. Since the functionalization reduced the pore size of UiO-Phe and -Me2, the benzene and toluene adsorption behaviors varied with different pressures. As shown in Figure 5, the simulated isotherms of benzene and toluene were similar in a two-stage shape but varied in saturated capacity on each UiO framework. The adsorption uptakes of UiO-Phe and UiO-Me2 increased sharply at relatively low pressures (0.1 kPa for benzene and 0.01 kPa for toluene, respectively), while that of UiO-67 transcended the two functional analogues at higher pressures. It should be mentioned that the adsorption uptakes of UiO-Phe and UiO-Me2 at low pressures could reach to a comparative level, despite that the S_{acc} and V_g of UiO-Phe were larger than UiO-Me2 (Table 1). Since the functionalization greatly contributed to the adsorption at low pressures, the effects of functional groups on the isosteric heats of adsorption were further discussed in Supporting Information, Figure S6. The results suggested that the adsorption was not only influenced by the textural properties of UiO-Phe and UiO-Me2, but the interaction strength between adsorbate and adsorbent was likely to affect the adsorption. As the pressure rose, the adsorption uptakes increased, and the tendency was in correspondence with the order of the S_{acc} and V_g of UiOs, suggesting the adsorption turned out to be structure-dependent at high pressures, similar to the adsorption on UiO-66, -67, and -68.

In addition, Shearer et al.[29] experimentally indicated that UiO-67 can not only undergo dehydration reversibly but can also exist in the intermediate form (singly dehydrated) for a finite time. Besides, they suggested that the stoichiometrical imperfection of the real UiO samples resulted from the substitution of the μ_3-OH groups on some Zr clusters by the chloride, with a Zr/Cl atomic ratio of 6:1. Therefore, apart from the ideal fully dehydrated models, we also compared the fully hydrated, singly dehydrated, and chloride-replaced models in the adsorption of benzene, so as to expand our simulated results to realistic materials. The calculated results are shown in Figure 6, while the configurations of different models were illustrated in Supporting Information, Figure S7. In the case of UiO-67, the adsorption on varied models exhibited analogous behaviors. However, the adsorbed amount on the fully hydrated, singly dehydrated as well as the chloride-replaced models of both UiO-Phe and UiO-Me2 were greater than that on the fully dehydrated model in the low-pressure range (0–0.11 kPa), similar to the adsorption of CO_2 on the hydrated and dehydrated UiO-66.[72] The calculated results suggested that the presence of μ_3-OH groups or chloride in UiO-Phe and

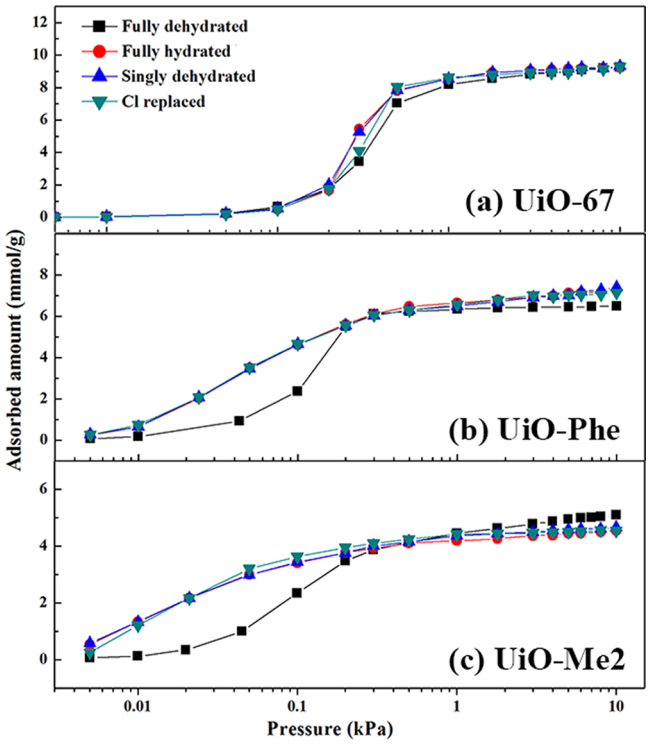

Figure 6. Adsorption isotherms of benzene on (a) UiO-67, (b) UiO-Phe and (c) UiO-Me2 with fully dehydrated, fully hydrated, singly dehydrated, and chloride-replaced models at 330 K.

-Me2 was capable of enhancing the adsorption. A plausible explanation lied in the functionalization that was likely to contribute to the interaction strength between adsorbate molecules and the μ_3-OH groups or chloride. It should be mentioned that since only one type of Zr cluster model was symmetrically distributed in a framework, the effects of multiple cluster models were difficult to examine and can be further studied in future work. In addition, it is more worthwhile to study a less complex scenario where all the Zr-MOFs are set as fully dehydrated to eliminate the effects of μ_3-OH groups, to exclusively investigate the influence of functionalization in this study.

To further investigate the effects of ligand-based functionalization on the adsorption of aromatics, the favorable adsorption locations of benzene on dehydrated UiO-Phe, UiO-Me2, and the original UiO-67 at 330 K were simulated and predicted. The density distribution of benzene in the (001) plane of UiO-67, -Phe, and -Me2 was obtained by accumulating the center of mass of benzene molecules with 1000 equilibrium configurations, as shown in Figure 7. The cases of toluene were similar to that of benzene (as shown in Supporting Information, Figure S8).

In the case of UiO-67, benzene preferentially adsorbed in the tetrahedral cages at low pressures, indicating the benzene molecules were more likely to be encapsulated inside the limited space of the cages. Meanwhile, the adsorption tended to occur around the ligands, revealing the strong adsorption affinity of benzene with the aromatic rings of ligands, similar to benzene adsorption on zeolite NaX and UiO-66.[18] When the pressures were higher than 0.1 kPa, benzene molecules started accessing the large octahedral cages after fully filling the small tetrahedral cages, corresponding to the quick rise in the isotherms (as shown in Figure 5a). At ~3 kPa, the octahedral

DOI: 10.1021/am508570d
ACS Appl. Mater. Interfaces 2015, 7, 5775–5787

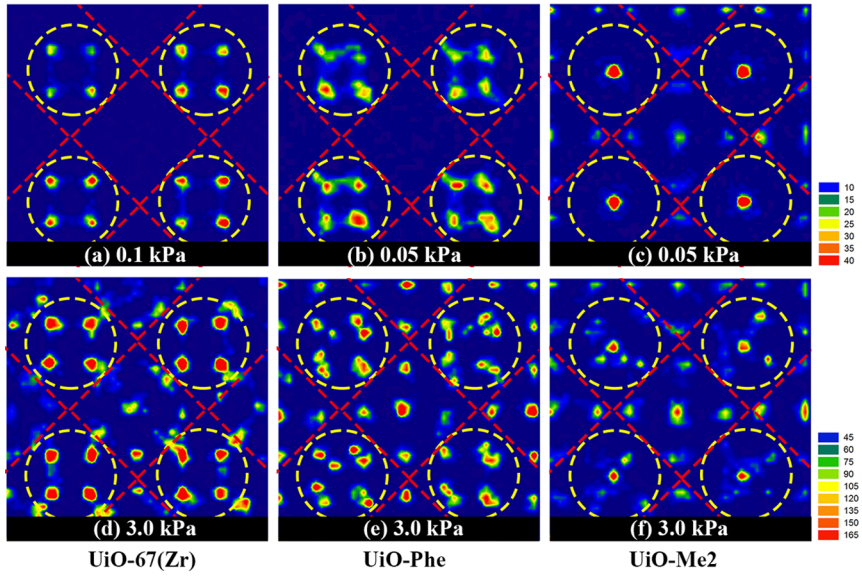

Figure 7. Density distribution contours for the center of mass of benzene in the (001) plane of UiO-67, UiO-Phe, and UiO-Me2 at (a, b, c) low and (d, e, f) high pressures. Dashed lines: yellow = tetrahedral cages; red = octahedral cages.

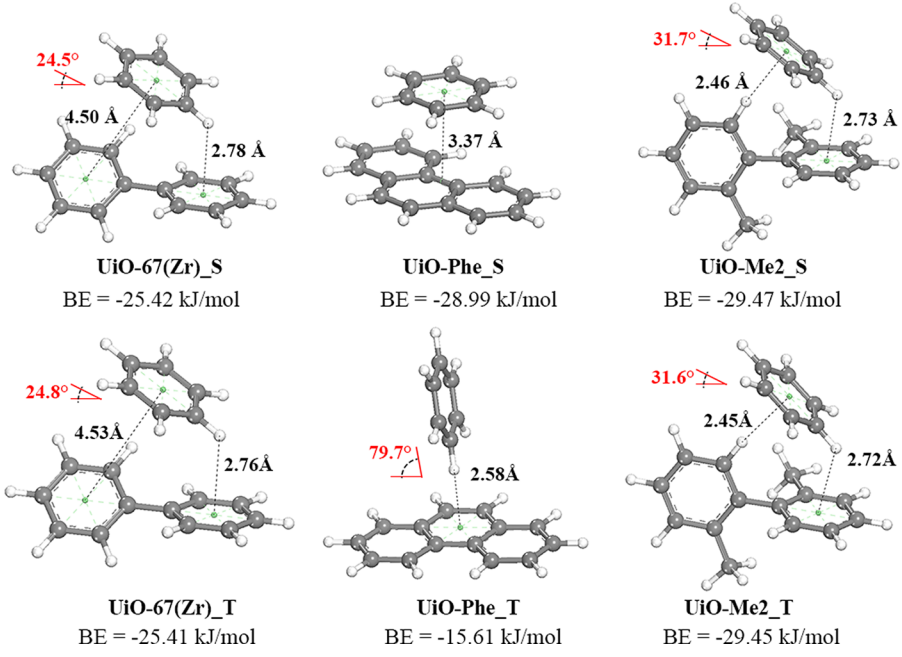

Figure 8. DFT-optimized adsorption complexes of benzene-linkers with S-shaped (upper) and T-shaped (lower) configurations on UiO-67, -Phe, and -Me2, with the binding energies.

cages were nearly saturated with benzene molecules; nevertheless, the dominant adsorption sites were still focused on tetrahedral cages, as illustrated in Figure 7d. Such observation of the sequential adsorption gives a reasonable explanation to the two-stage isotherms of benzene adsorption on UiOs, similar to methanol adsorption on Cu-BTC.[66]

In terms of adsorption behaviors, variations were found on UiO-Phe and UiO-Me2 compared to UiO-67. At low pressures, UiO-Phe showed a larger area of local density at the linkers of tetrahedral cages than UiO-67 (as shown in Figure 7b), suggesting the significant benefits of spacious space in cages coming from the larger ligands. For UiO-Me2, the adsorbed benzene molecules were centralized at the tetrahedral cages (see Figure 7c). The adsorption behavior could be associated with the steric hindrance effects that resulted from the additional methyl groups as well as the rotation of aromatic rings in the linkers. At higher pressure of 3 kPa, pronounced adsorption sites in the octahedral cages of UiO-Phe and -Me2 were observed, indicating that the insertion of functional groups was capable of generating new adsorption sites at higher pressures. However, the final value of local densities decreased with S_{acc} and V_g, following the order of UiO-67 > UiO-Phe > UiO-Me2, which revealed that the adsorption at high pressures was still governed by the structural properties of the frameworks. Thus, these results suggested that the functionalization by incorporating the linkers with additional aromatic ring (UiO-Phe) and methyl groups (UiO-Me2) were promising

DOI: 10.1021/am508570d
ACS Appl. Mater. Interfaces 2015, 7, 5775−5787

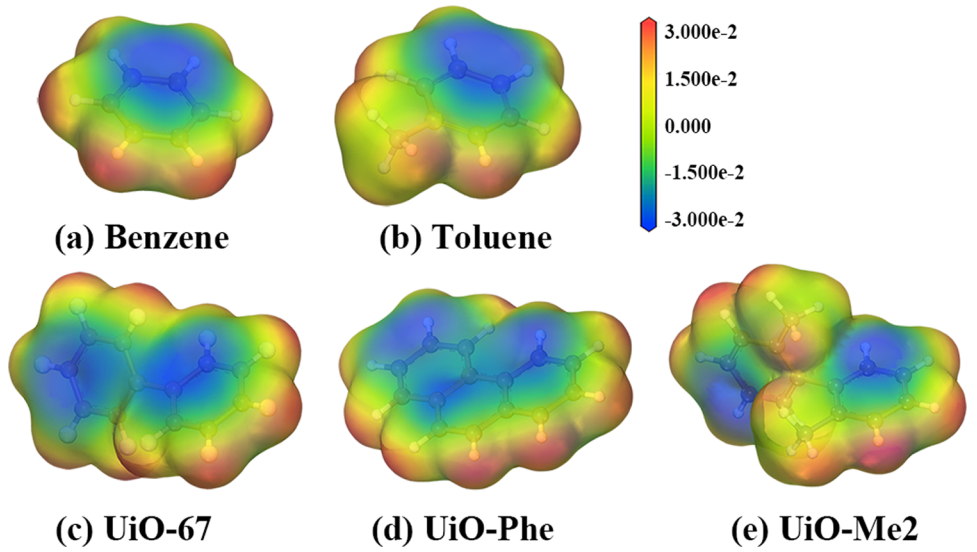

Figure 9. Electrostatic potential maps around (a) benzene and (b) toluene, the organic linkers of (c) UiO-67, (d) UiO-Phe, and (e) UiO-Me2.

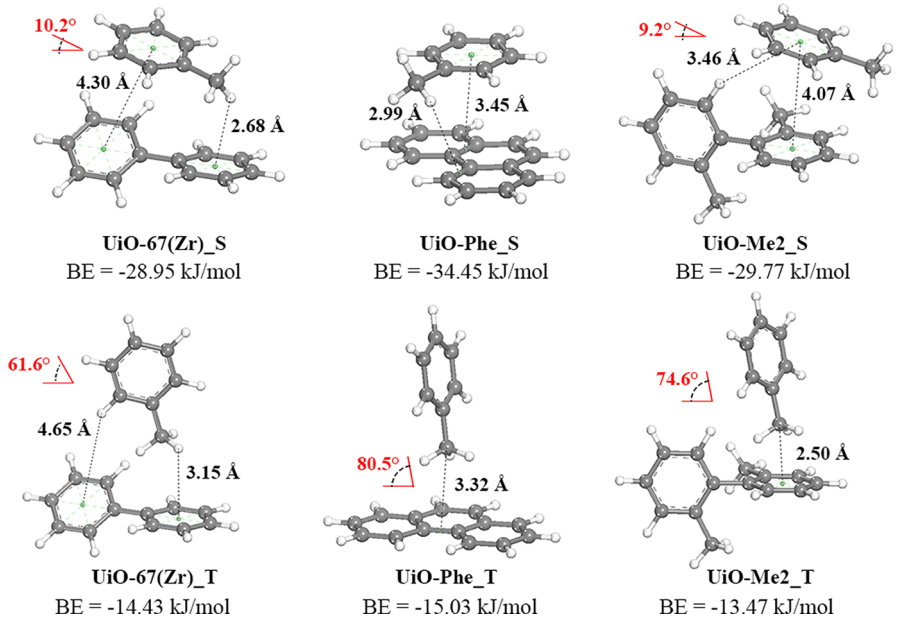

Figure 10. DFT-optimized adsorption complexes of toluene-linkers with S-shaped (upper) and T-shaped (lower) configurations on UiO-67, -Phe, and -Me2, with the corresponding binding energies.

approaches to improve the adsorption performance of aromatics at lower pressures.

3.3. Adsorption Thermodynamics. DFT calculation was employed to obtain the energy-minimum configurations and the corresponding binding energies (BEs) between aromatics and the frameworks (UiO-67, -Phe, and -Me2). Previous works experimentally studied the UiO materials using thermogravimetric analysis and found that there were missing linkers in the as-made samples, leading to the presence of strong adsorption sites (Lewis acid sites).[29,73] Therefore, apart from fully hydrated and dehydrated Zr clusters, we also constructed a deficient cluster with one linker missing, and the deficient vacancy was terminated by chloride, as suggested by Shearer et al.[29,74] The BEs of benzene at these three types of Zr clusters were calculated, and the results were shown in Supporting Information, Figure S9. Since the ideal hydrated and dehydrated clusters were surrounded by 12 carboxylate linkers, the adsorption affinity was relatively weak (−10 to ca. −16 kJ/mol) due to the steric constrains. By contrast, the linker deficiency in Zr cluster led to stronger available adsorption sites (−22.06 kJ/mol) and enhanced pore accessibility for large molecules when compared to the 12-connected cluster. However, the decreased connectivity of Zr-MOFs also results in the change of framework topology and the lower BET area,[75] which may cause drawbacks for the adsorption.

In the case of organic linkers, two major configurations of adsorption complexes, namely, the parallel face-to-face stacking "sandwich" (S-shaped) and the perpendicular T-shaped geometries (as shown in Supporting Information, Figures S10 and Figure S11), were examined. Previous calculations using ab initio methods have shown that both the configurations were favorable between benzene molecules arranged in dimers and trimers,[76] which were prone to form $\pi-\pi$ overlap dispersion

DOI: 10.1021/am508570d
ACS Appl. Mater. Interfaces 2015, 7, 5775−5787

with S-shaped geometry and electrostatic interactions with T-shaped orientation,[77,78] respectively.

Figure 8 showed the BEs of benzene in all the complexes with S-shaped configuration were more exothermic than those with T-shape on each UiO material, suggesting the $\pi-\pi$ stacking interactions rather than the T-shaped electrostatic interactions dominated the adsorption, coinciding with the interaction behaviors of benzene dimers reported by Headen et al.[79] It was noticeable that benzene molecules in both UiO-67 and UiO-Me2 shifted to an intermediate position between S-shaped and T-shaped conformations, suggesting both conjugated π system and electrostatic interaction contributed to the adsorption of benzene. UiO-Me2 showed a greater adsorption affinity (−29.47 kJ/mol) than UiO-67 (−25.42 kJ/mol), indicating the addition of methyl groups had beneficial effects on the adsorbate-framework interaction. In the case of UiO-Phe, the enlarged aromatic rings promoted larger and more continuous π-orbital delocalization compared to UiO-67, as shown in the electrostatic potentials in Figure 9, which could also enhance the $\pi-\pi$ stacking interaction strength (−28.99 kJ/mol).

The adsorption at low pressures was likely to be controlled by either adsorbate−adsorbent interactions (energetic effects) or textural properties of the framework (entropic effects), or both, depending on the relative strength of each. UiO-Phe and UiO-Me2 possessed similar adsorption uptakes at low pressures, following the order of UiO-Phe ≈ UiO-Me2 > UiO-67 (Figure 5a), which coincided well with the order of BEs on the UiOs, regardless of the variation in V_g and S_{acc}. It suggested that unlike the adsorption on UiO-66, -67, and -68, the smaller pore size of UiO-Phe and -Me2 was not necessary to provide a strong binding to benzene at low pressures, since the energetic effects caused by the presence of functional groups have greater contribution to the adsorption of benzene.

The optimized configurations of toluene-linker complexes were demonstrated in Figure 10. As evidenced by the higher value of BEs, the $\pi-\pi$ stacking interaction was still thermodynamically favorable by toluene, similar to the adsorption of benzene. However, different from benzene, the presence of the methyl group in toluene acted as both electron donor to strengthen the π system and as a steric hindrance to weaken the interaction. Toluene with S-shaped geometries showed higher interaction affinity on all the three UiOs compared to benzene accordingly, suggesting the electron-donating effect was slightly stronger than the steric hindrance effect of the methyl group in toluene on the adsorption. In addition, the BE of toluene with S-shaped configuration on UiO-Phe (−34.45 kJ/mol) increased by 5.46 kJ/mol from a lower value (−28.99 kJ/mol) of benzene, which held the highest increment of interaction energy compared to UiO-67 (3.53 kJ/mol) and UiO-Me2 (0.30 kJ/mol). It indicated that the addition of aromatic ring on linker made the framework more favorable for interacting with toluene, which could probably contribute to the separation of toluene/benzene mixtures, whereas the functionalization of UiO-Me2 might have negative effects on the separation, as the functionalization diminished the difference in BEs between toluene and benzene.

On the other hand, the larger inclined angles of toluene with T-shaped geometries on UiOs compared to benzene indicated that the electrostatic interaction became a dominant driving force for the adsorption. Meanwhile, the BEs of T-shaped toluene were less exothermic than benzene, revealing that the electrostatic interaction was restricted by the methyl group of toluene. It can be ascribed to the weaker electropositivity of methyl group in toluene that cannot offer sufficient interaction with the frameworks compared to the H atoms of benzene, as shown in ESPs of benzene and toluene in Figure 9a,b. The BE of toluene on UiO-Phe (−15.03 kJ/mol) was stronger than those of UiO-67 (−14.43 kJ/mol) and -Me2 (−13.47 kJ/mol), suggesting that the additional aromatic ring in the linker of UiO-Phe was capable of preventing the adsorbate−adsorbent interactions from the negative effects caused by methyl group in toluene.

Although the methyl group in toluene has varied effects on the adsorption in S-shaped and T-shaped configurations, the BEs of toluene with favorable orientation still increased with the adsorption uptakes at low pressures (Figure 5b), similar to the case of benzene, which further consolidated the predominant role of energetic effect in the low-pressure adsorption.

3.4. Adsorption Selectivity for Toluene/Benzene Mixtures. IAST calculations based on DSLF model were performed to predict the adsorption selectivities of toluene/benzene equimolar mixtures on UiO-67, -68, -Phe, and -Me2, as shown in Figure 11. The selectivity on UiO-68 was compared with that of UiO-Phe, as both contain three aromatic rings in each linker but varied in the pore sizes.

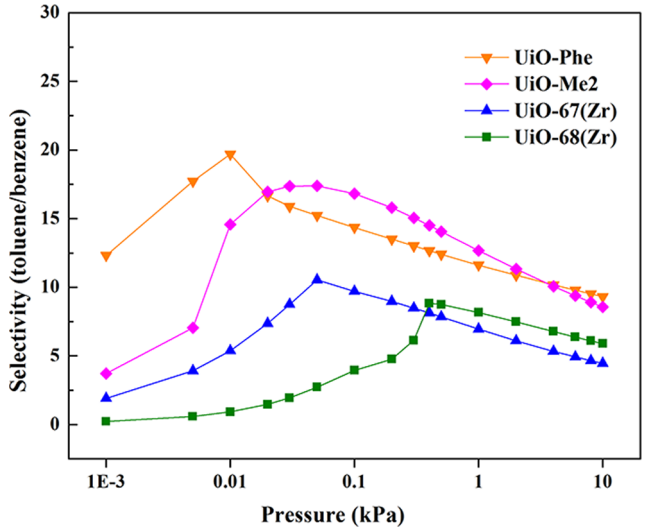

Figure 11. Adsorption selectivities predicted by IAST for equimolar mixtures of toluene/benzene as a function of total bulk pressures at 330 K.

It could be found that two stages were present on the toluene selectivity curves for all the UiOs. A rapid increase in toluene selectivities first appeared at low pressures, followed by a linear decrease as pressures continued to rise, and the maximal selectivities followed the order of UiO-Phe > UiO-Me2 > UiO-67 > UiO-68. Although the highest selectivities appeared at relatively low pressures, there are still effective for practical separation process as these aromatics are generally very dilute in most industrial applications.[24]

We believed that the factors affecting the selectivity vary with different pressure ranges. As mentioned earlier, the adsorption at lower pressures was governed by the $\pi-\pi$ stacking interactions, in which toluene possessed greater adsorption affinity than benzene, leading to a sharp increase in toluene selectivity, while the effects of steric hindrance hold up the

DOI: 10.1021/am508570d
ACS Appl. Mater. Interfaces 2015, 7, 5775−5787

adsorption once the pores and cages of UiOs were saturated by adsorbates at higher pressures, and the smaller size of benzene molecules allowed further access to the cages as pressures rose, which made a consistent decrease in the selectivity. On the other hand, UiO-Phe showed maximum value of toluene selectivity, reflecting the introduction of additional aromatic rings to the ligand furnished appropriate adsorption interaction strength and suitable V_g and S_{acc}, which provided significant benefits for the separation process. UiO-Me2 possessed lower selectivity as the methyl groups in linkers brought about stronger negative effects of steric hindrance to the separation, while the largest V_g and S_{acc} of UiO-68 led to the lowest selectivity.

We also investigated the influence of toluene concentrations on toluene selectivity at the low pressure of 0.01 kPa, as shown in Figure 12, since the separation in dilute conditions is more

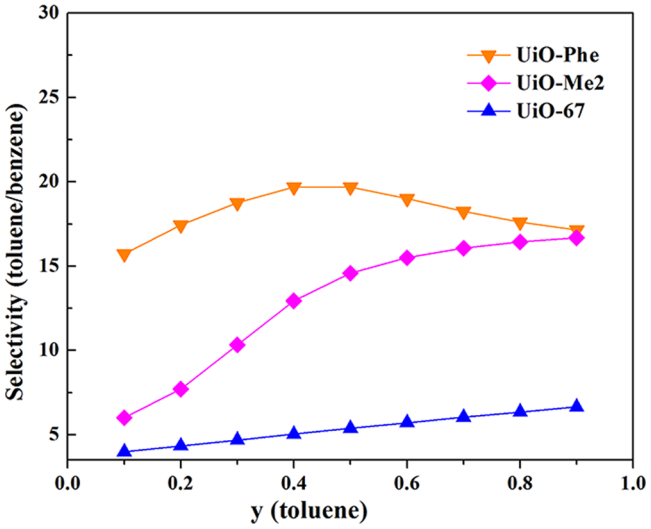

Figure 12. Toluene selectivity vs the gas mole fraction of toluene in the mixtures at 330 K and 0.01 kPa.

valuable for practical applications. It was interesting to find that the tendency of selectivity varied with different UiOs. Toluene selectivity on UiO-67 increased linearly with gas mole fraction of toluene, while the selectivity grew slowly in the case of UiO-Me2. Unlike UiO-67 and -Me2, UiO-Phe expressed a maximum value of selectivity in equimolar mixtures. The varied trends of selectivity were probably ascribed to the counterbalancing factors of adsorbate−adsorbent interactions and suitable textural properties (pore size, S_{acc}) of the frameworks. However, in the measured range of toluene concentrations, the selectivity on UiO-Phe maintained a relatively high value compared to that of UiO-Me2 and -67, suggesting that the functionalization with additional aromatic rings is the most promising strategy to enhance toluene selectivity.

4. CONCLUSION

Adsorption and separation properties of toluene and benzene on UiO materials were studied by multiscale simulation approach combining GCMC, DFT, and IAST methods. In this work, two new types of UiOs (UiO-Phe and -Me2) were constructed by grafting additional aromatic rings and methyl groups to the linkers of UiO-67. Both UiO-Phe and -Me2 can efficiently increase the adsorption uptakes at low pressures compared to their parent UiO-67, majorly by decreasing the pore size and strengthening the interaction affinity with the adsorbates. While at high pressures, the larger pore volume and surface turn out to play predominant roles in the adsorption. UiO-Phe possesses higher capacity than UiO-Me2, as the former suffers less steric hindrance effects. Additionally, the single-component adsorption isotherms on UiOs show a two-stage adsorption behavior at the measured pressure ranges, which can be ascribed to the sequential adsorption mechanics in varied cages of the frameworks. In terms of toluene/benzene separation, the IAST predicted maximal toluene selectivities can be reached at a certain pressure, associating with the counterbalancing influences of adsorbte−framework interaction strength and suitable pore size. UiO-Phe has the highest adsorption capacity and toluene selectivity at low pressures, suggesting the functionalization of linkers with additional aromatic rings is effective to improve adsorption and separation performance for toluene/benzene mixtures. The present work provides valuable insights into the effects of ligand functionalization on aromatic adsorption and separation using a simulation approach, which could guide the rational experiment design of highly efficient UiO adsorbent for the adsorption and separation of aromatic compounds.

■ ASSOCIATED CONTENT

Supporting Information

Models for toluene and benzene, atomic types of UiOs, LJ potential parameters and partial charges for adsorbates and UiOs, the fitting parameters of DSLF model, adsorption isotherms on UiOs, optimized structures of UiO linkers, isosteric heats of adsorption, different models of Zr clusters, the density distribution contours of toluene, and the initial complexes of benzene and toluene adsorbing onto the UiO linkers. This material is available free of charge via the Internet at http://pubs.acs.org.

■ AUTHOR INFORMATION

Corresponding Author

*Phone: 86-13825124468. Fax: 86-020-87113735. E-mail: cehxxi@scut.edu.cn.

Notes

The authors declare no competing financial interest.

■ ACKNOWLEDGMENTS

We gratefully acknowledge the financial support from the National Natural Science Foundation of China (Nos. 21436005 and 21176084), the National High Technology Research and Development Program of China (No. 2013AA065005), Specialized Research Fund for the Doctoral Program of Higher Education of China (No. 20130172110012), and Guangdong Natural Science Foundation (S2011 030001366).

■ REFERENCES

(1) Planchais, A.; Devautour-Vinot, S.; Giret, S.; Salles, F.; Trens, P.; Fateeva, A.; Devic, T.; Yot, P.; Serre, C.; Ramsahye, N.; Maurin, G. Adsorption of Benzene in the Cation-Containing MOFs MIL-141. *J. Phys. Chem. C* **2013**, *117*, 19393−19401.

(2) Canet, X.; Gilles, F.; Su, B. L.; de Weireld, G.; Frère, M. Adsorption of Alkanes and Aromatic Compounds on Various Faujasites in the Henry Domain. 1. Compensating Cation Effect on Zeolites Y. *J. Chem. Eng. Data* **2007**, *52*, 2117−2126.

(3) Zaitan, H.; Korrir, A.; Chafik, T.; Bianchi, D. Evaluation of the Potential of Volatile Organic Compound (Di-Methyl Benzene)

DOI: 10.1021/am508570d
ACS Appl. Mater. Interfaces 2015, 7, 5775−5787

Removal Using Adsorption on Natural Minerals Compared to Commercial Oxides. *J. Hazard. Mater.* **2013**, *262*, 365−376.
(4) Wu, L.; Sitamraju, S.; Xiao, J.; Liu, B.; Li, Z.; Janik, M. J.; Song, C. Effect of Liquid-Phase O_3 Oxidation of Activated Carbon on the Adsorption of Thiophene. *Chem. Eng. J.* **2014**, *242*, 211−219.
(5) Guvenc, E.; Ahunbay, M. G. Adsorption of Methyl Tertiary Butyl Ether and Trichloroethylene in MFI-Type Zeolites. *J. Phys. Chem. C* **2012**, *116*, 21836−21843.
(6) Zhang, W.; Qu, Z.; Li, X.; Wang, Y.; Ma, D.; Wu, J. Comparison of Dynamic Adsorption/Desorption Characteristics of Toluene on Different Porous Materials. *J. Environ. Sci.* **2012**, *24*, 520−528.
(7) Baek, S. W.; Kim, J. R.; Ihm, S. K. Design of Dual Functional Adsorbent/Catalyst System for the Control of VOC's by Using Metal-Loaded Hydrophobic Y-Zeolites. *Catal. Today* **2004**, *93*−*95*, 575−581.
(8) Zeng, Y.; Zhu, X.; Yuan, Y.; Zhang, X.; Ju, S. Molecular Simulations for Adsorption and Separation of Thiophene and Benzene in Cu-BTC and IRMOF-1 Metal−Organic Frameworks. *Sep. Purif. Technol.* **2012**, *95*, 149−156.
(9) Wu, Y.; Xiao, J.; Wu, L.; Chen, M.; Xi, H.; Li, Z.; Wang, H. Adsorptive Denitrogenation of Fuel over Metal Organic Frameworks: Effect of N-Types and Adsorption Mechanisms. *J. Phys. Chem. C* **2014**, *118*, 22533−22543.
(10) Hasan, Z.; Jhung, S. H. Removal of Hazardous Organics from Water Using Metal-Organic Frameworks (MOFs): Plausible Mechanisms for Selective Adsorptions. *J. Hazard. Mater.* **2015**, *283*, 329−339.
(11) Jia, S. Y.; Zhang, Y. F.; Liu, Y.; Qin, F. X.; Ren, H. T.; Wu, S. H. Adsorptive Removal of Dibenzothiophene from Model Fuels over One-Pot Synthesized PTA@MIL-101(Cr) Hybrid Material. *J. Hazard. Mater.* **2013**, *262*, 589−597.
(12) Han, S.; Huang, Y.; Watanabe, T.; Dai, Y.; Walton, K. S.; Nair, S.; Sholl, D. S.; Meredith, J. C. High-Throughput Screening of Metal−Organic Frameworks for CO_2 Separation. *ACS Comb. Sci.* **2012**, *14*, 263−267.
(13) Wu, L.; Xiao, J.; Wu, Y.; Xian, S.; Miao, G.; Wang, H.; Li, Z. A Combined Experimental/Computational Study on the Adsorption of Organosulfur Compounds over Metal-Organic Frameworks from Fuels. *Langmuir* **2014**, *30*, 1080−1088.
(14) Cavka, J. H.; Jakobsen, S.; Olsbye, U.; Guillou, N.; Lamberti, C.; Bordiga, S.; Lillerud, K. P. A New Zirconium Inorganic Building Brick Forming Metal Organic Frameworks with Exceptional Stability. *J. Am. Chem. Soc.* **2008**, *130*, 13850−13851.
(15) Jasuja, H.; Zang, J.; Sholl, D. S.; Walton, K. S. Rational Tuning of Water Vapor and CO_2 Adsorption in Highly Stable Zr-Based MOFs. *J. Phys. Chem. C* **2012**, *116*, 23526−23532.
(16) Colon, Y. J.; Krishna, R.; Snurr, R. Q. Strong Influence of the H_2 Binding Energy on the Maxwell-Stefan Diffusivity in Nu-100, UiO-68, and IRMOF-16. *Microporous Mesoporous Mater.* **2014**, *185*, 190−196.
(17) Wu, D.; Maurin, G.; Yang, Q.; Serre, C.; Jobic, H.; Zhong, C. Computational Exploration of a Zr-Carboxylate Based Metal-Organic Framework as a Membrane Material for CO_2 Capture. *J. Mater. Chem. A* **2014**, *2*, 1657−1661.
(18) Ramsahye, N. A.; Trens, P.; Shepherd, C.; Gonzalez, P.; Trung, T. K.; Ragon, F.; Serre, C. The Effect of Pore Shape on Hydrocarbon Selectivity on UiO-66(Zr), HKUST-1 and MIL-125(Ti) Metal Organic Frameworks: Insights from Molecular Simulations and Chromatography. *Microporous Mesoporous Mater.* **2014**, *189*, 222−231.
(19) Pinto, M. L.; Dias, S.; Pires, J. Composite MOF Foams: The Example of UiO-66/Polyurethane. *ACS Appl. Mater. Interfaces* **2013**, *5*, 2360−2363.
(20) Na, C.; Yan, X. P. Exploring Reverse Shape Selectivity and Molecular Sieving Effect of Metal-Organic Framework UiO-66 Coated Capillary Column for Gas Chromatographic Separation. *J. Chromatogr., A* **2012**, *1257*, 116−124.
(21) Feng, D.; Gu, Z. Y.; Chen, Y. P.; Park, J.; Wei, Z.; Sun, Y.; Bosch, M.; Yuan, S.; Zhou, H. C. A Highly Stable Porphyrinic Zirconium Metal−Organic Framework with shp-a Topology. *J. Am. Chem. Soc.* **2014**, *136*, 17714−17717.
(22) DeCoste, J. B.; Peterson, G. W.; Jasuja, H.; Glover, T. G.; Huang, Y. g.; Walton, K. S. Stability and Degradation Mechanisms of Metal-Organic Frameworks Containing the $Zr_6O_4(OH)_4$ Secondary Building Unit. *J. Mater. Chem. A* **2013**, *1*, 5642−5650.
(23) Zhang, M.; Chen, Y. P.; Bosch, M.; Gentle, T.; Wang, K.; Feng, D.; Wang, Z. U.; Zhou, H. C. Symmetry-Guided Synthesis of Highly Porous Metal−Organic Frameworks with Fluorite Topology. *Angew. Chem., Int. Ed.* **2014**, *53*, 815−818.
(24) Lillo-Rodenas, M. A.; Fletcher, A. J.; Thomas, K. M.; Cazorla-Amoros, D.; Linares-Solano, A. Competitive Adsorption of a Benzene-Toluene Mixture on Activated Carbons at Low Concentration. *Carbon* **2006**, *44*, 1455−1463.
(25) Duerinck, T.; Bueno-Perez, R.; Vermoortele, F.; De Vos, D. E.; Calero, S.; Baron, G. V.; Denayer, J. F. M. Understanding Hydrocarbon Adsorption in the UiO-66 Metal-Organic Framework: Separation of (Un)Saturated Linear, Branched, Cyclic Adsorbates, Including Stereoisomers. *J. Phys. Chem. C* **2013**, *117*, 12567−12578.
(26) Chun, J.; Kang, S.; Park, N.; Park, E. J.; Jin, X.; Kim, K. D.; Seo, H. O.; Lee, S. M.; Kim, H. J.; Kwon, W. H.; Park, Y. K.; Kim, J. M.; Kim, Y. D.; Son, S. U. Metal-Organic Framework@Microporous Organic Network: Hydrophobic Adsorbents with a Crystalline Inner Porosity. *J. Am. Chem. Soc.* **2014**, *136*, 6786−6789.
(27) Lau, C. H.; Babarao, R.; Hill, M. R. A Route to Drastic Increase of CO_2 Uptake in Zr Metal Organic Framework UiO-66. *Chem. Commun.* **2013**, *49*, 3634−3636.
(28) Ko, D.; Kim, M.; Moon, I.; Choi, D. k. Analysis of Purge Gas Temperature in Cyclic TSA Process. *Chem. Eng. Sci.* **2002**, *57*, 179−195.
(29) Shearer, G.; Forselv, S.; Chavan, S.; Bordiga, S.; Mathisen, K.; Bjørgen, M.; Svelle, S.; Lillerud, K. In Situ Infrared Spectroscopic and Gravimetric Characterisation of the Solvent Removal and Dehydroxylation of the Metal Organic Frameworks UiO-66 and UiO-67. *Top. Catal.* **2013**, *56*, 770−782.
(30) *Materials Studio 5.0;* Accelrys: San Diego, CA, 2010.
(31) Martin, M. G.; Siepmann, J. I. Novel Configurational-Bias Monte Carlo Method for Branched Molecules. Transferable Potentials for Phase Equilibria. 2. United-Atom Description of Branched Alkanes. *J. Phys. Chem. B* **1999**, *103*, 4508−4517.
(32) Wick, C. D.; Siepmann, J. I.; Klotz, W. L.; Schure, M. R. Temperature Effects on the Retention of N-Alkanes and Arenes in Helium−Squalane Gas−Liquid Chromatography: Experiment and Molecular Simulation. *J. Chromatogr., A* **2002**, *954*, 181−190.
(33) Zhao, X. S.; Chen, B.; Karaborni, S.; Siepmann, J. I. Vapor−Liquid and Vapor−Solid Phase Equilibria for United-Atom Benzene Models near Their Triple Points: The Importance of Quadrupolar Interactions. *J. Phys. Chem. B* **2005**, *109*, 5368−5374.
(34) Wick, C. D.; Martin, M. G.; Siepmann, J. I. Transferable Potentials for Phase Equilibria. 4. United-Atom Description of Linear and Branched Alkenes and Alkylbenzenes. *J. Phys. Chem. B* **2000**, *104*, 8008−8016.
(35) Nieto-Draghi, C.; Bonnaud, P.; Ungerer, P. Anisotropic United Atom Model Including the Electrostatic Interactions of Methylbenzenes. I. Thermodynamic and Structural Properties. *J. Phys. Chem. C* **2007**, *111*, 15686−15699.
(36) Peralta, D.; Barthelet, K.; Perez-Pellitero, J.; Chizallet, C.; Chaplais, G.; Simon-Masseron, A.; Pirngruber, G. D. Adsorption and Separation of Xylene Isomers: CPO-27-Ni Vs HKUST-1 Vs NaY. *J. Phys. Chem. C* **2012**, *116*, 21844−21855.
(37) Banu, A. M.; Friedrich, D.; Brandani, S.; Dueren, T. A Multiscale Study of MOFs as Adsorbents in H_2 PSA Purification. *Ind. Eng. Chem. Res.* **2013**, *52*, 9946−9957.
(38) Wu, D.; Yang, Q.; Zhong, C.; Liu, D.; Huang, H.; Zhang, W.; Maurin, G. Revealing the Structure−Property Relationships of Metal−Organic Frameworks for CO_2 Capture from Flue Gas. *Langmuir* **2012**, *28*, 12094−12099.
(39) Xu, Q.; Zhong, C. A General Approach for Estimating Framework Charges in Metal−Organic Frameworks. *J. Phys. Chem. C* **2010**, *114*, 5035−5042.

DOI: 10.1021/am508570d
ACS Appl. Mater. Interfaces 2015, 7, 5775−5787

(40) Frisch, M. J.; Trucks, G. W.; Schlegel, H. B.; Scuseria, G. E.; Robb, M. A.; Cheeseman, J. R.; Scalmani, G.; Barone, V.; Mennucci, B.; Petersson, G. A.; Nakatsuji, H.; Caricato, M.; Li, X.; Hratchian, H. P.; Izmaylov, A. F.; Bloino, J.; Zheng, G.; Sonnenberg, J. L.; Hada, M.; Ehara, M.; Toyota, K.; Fukuda, R.; Hasegawa, J.; Ishida, M.; Nakajima, T.; Honda, Y.; Kitao, O.; Nakai, H.; Vreven, T.; Montgomery, J. A., Jr.; Peralta, J. E.; Ogliaro, F.; Bearpark, M.; Heyd, J. J.; Brothers, E.; Kudin, K. N.; Staroverov, V. N.; Kobayashi, R.; Normand, J.; Raghavachari, K.; Rendell, A.; Burant, J. C.; Iyengar, S. S.; Tomasi, J.; Cossi, M.; Rega, N.; Millam, M. J.; Klene, M.; Knox, J. E.; Cross, J. B.; Bakken, V.; Adamo, C.; Jaramillo, J.; Gomperts, R.; Stratmann, R. E.; Yazyev, O.; Austin, A. J.; Cammi, R.; Pomelli, C.; Ochterski, J. W.; Martin, R. L.; Morokuma, K.; Zakrzewski, V. G.; Voth, G. A.; Salvador, P.; Dannenberg, J. J.; Dapprich, S.; Daniels, A. D.; Farkas, Ö.; Foresman, J. B.; Ortiz, J. V.; Cioslowski, J.; Fox, D. J. *Gaussian 09*, Revision D. 01; Gaussian, Inc.: Wallingford, CT, 2009.

(41) Keskin, S. Atomistic Simulations for Adsorption, Diffusion, and Separation of Gas Mixtures in Zeolite Imidazolate Frameworks. *J. Phys. Chem. C* **2010**, *115*, 800−807.

(42) Trens, P.; Belarbi, H.; Shepherd, C.; Gonzalez, P.; Ramsahye, N. A.; Lee, U. H.; Seo, Y. K.; Chang, J. S. Adsorption and Separation of Xylene Isomers Vapors onto the Chromium Terephthalate-Based Porous Material MIL-101(Cr): An Experimental and Computational Study. *Microporous Mesoporous Mater.* **2014**, *183*, 17−22.

(43) Gupta, A.; Chempath, S.; Sanborn, M. J.; Clark, L. A.; Snurr, R. Q. Object-Oriented Programming Paradigms for Molecular Modeling. *Mol. Simul.* **2003**, *29*, 29−46.

(44) Cho, J.; Rho, S.; Park, S.; Lee, J.; Kim, H. A Comparison between Anderko's Model with Composition-Dependent Physical Interaction Parameters and SRK-Based Hexamer Model for HFC and HF Systems. *Fluid Phase Equilib.* **1998**, *144*, 69−75.

(45) Zhao, Q.; Yuan, W.; Liang, J.; Li, J. Synthesis and Hydrogen Storage Studies of Metal-Organic Framework UiO-66. *Int. J. Hydrogen Energy* **2013**, *38*, 13104−13109.

(46) Colón, Y. J.; Brand, S. K.; Snurr, R. Q. Effect of Metal Alkoxide Functionalization on Hydrogen Mobility in Metal−Organic Frameworks. *Chem. Phys. Lett.* **2013**, *577*, 76−81.

(47) Düren, T.; Snurr, R. Q. Assessment of Isoreticular Metal−Organic Frameworks for Adsorption Separations: A Molecular Simulation Study of Methane/N-Butane Mixtures. *J. Phys. Chem. B* **2004**, *108*, 15703−15708.

(48) Talu, O.; Myers, A. L. Molecular Simulation of Adsorption: Gibbs Dividing Surface and Comparison with Experiment. *AIChE J.* **2001**, *47*, 1160−1168.

(49) Snurr, R. Q.; Bell, A. T.; Theodorou, D. N. Prediction of Adsorption of Aromatic Hydrocarbons in Silicalite from Grand Canonical Monte Carlo Simulations with Biased Insertions. *J. Phys. Chem.* **1993**, *97*, 13742−13752.

(50) Wu, Y.; Chen, H.; Liu, D.; Qian, Y.; Xi, H. Adsorption and Separation of Ethane/Ethylene on ZIFs with Various Topologies: Combining GCMC Simulation with the Ideal Adsorbed Solution Theory (IAST). *Chem. Eng. Sci.* **2015**, *124*, 144−153.

(51) Zhang, Z.; Li, Z.; Li, J. Computational Study of Adsorption and Separation of CO_2, CH_4, and N_2 by an rht-Type Metal-Organic Framework. *Langmuir* **2012**, *28*, 12122−33.

(52) Zhang, Z.; Liu, J.; Li, Z.; Li, J. Experimental and Theoretical Investigations on the MMOF Selectivity for CO_2 Vs. N_2 in Flue Gas Mixtures. *Dalton Trans.* **2012**, *41*, 4232−4238.

(53) Mishra, P.; Mekala, S.; Dreisbach, F.; Mandal, B.; Gumma, S. Adsorption of CO_2, CO, CH_4, and N_2 on a Zinc Based Metal Organic Framework. *Sep. Purif. Technol.* **2012**, *94*, 124−130.

(54) Bae, Y. S.; Farha, O. K.; Spokoyny, A. M.; Mirkin, C. A.; Hupp, J. T.; Snurr, R. Q. Carborane-Based Metal-Organic Frameworks as Highly Selective Sorbents for CO_2 over Methane. *Chem. Commun.* **2008**, 4135−4137.

(55) Bae, Y. S.; Mulfort, K. L.; Frost, H.; Ryan, P.; Punnathanam, S.; Broadbelt, L. J.; Hupp, J. T.; Snurr, R. Q. Separation of CO_2 from CH_4 Using Mixed-Ligand Metal−Organic Frameworks. *Langmuir* **2008**, *24*, 8592−8598.

(56) Da, C. J.; Martin, H. G. Long-Range Corrected Hybrid Density Functionals with Damped Atom-Atom Dispersion Corrections. *Phys. Chem. Chem. Phys.* **2008**, *10*, 6615−6620.

(57) Wang, W.; Zhang, Y.; Wang, Y. B. Noncovalent Π···Π Interaction between Graphene and Aromatic Molecule: Structure, Energy, and Nature. *J. Chem. Phys.* **2014**, *140* (094302), 1−6.

(58) Sang Soo, H.; Dong Hyun, J.; Seung-Hoon, C.; Jiyoung, H. Lithium-Functionalized Metal-Organic Frameworks That Show >10 Wt % H_2 Uptake at Ambient Temperature. *ChemPhysChem* **2013**, *14*, 2698−703.

(59) Kim, K. C.; Yu, D.; Snurr, R. Q. Computational Screening of Functional Groups for Ammonia Capture in Metal−Organic Frameworks. *Langmuir* **2013**, *29*, 1446−1456.

(60) Kasuriya, S.; Namuangruk, S.; Treesukol, P.; Tirtowidjojo, M.; Limtrakul, J. Adsorption of Ethylene, Benzene, and Ethylbenzene over Faujasite Zeolites Investigated by the Oniom Method. *J. Catal.* **2003**, *219*, 320−328.

(61) Boys, S. F.; Bernardi, F. The Calculation of Small Molecular Interactions by the Differences of Separate Total Energies. Some Procedures with Reduced Errors. *Mol. Phys.* **1970**, *19*, 553−566.

(62) Xiao, J.; Sitamraju, S.; Janik, M. J. CO_2 Adsorption Thermodynamics over N-Substituted/Grafted Graphanes: A DFT Study. *Langmuir* **2014**, *30*, 1837−1844.

(63) Rouquerol, J.; Rouquerol, F.; Llewellyn, P.; Maurin, G.; Sing, K. S. *Adsorption by Powders and Porous Solids: Principles, Methodology, and Applications,* 2nd ed.; Academic Press: London, U.K., 2013.

(64) Chavan, S.; Vitillo, J. G.; Gianolio, D.; Zavorotynska, O.; Civalleri, B.; Jakobsen, S.; Nilsen, M. H.; Valenzano, L.; Lamberti, C.; Lillerud, K. P.; Bordiga, S. H_2 Storage in Isostructural UiO-67 and UiO-66 MOFs. *Phys. Chem. Chem. Phys.* **2012**, *14*, 1614−1626.

(65) Getman, R. B.; Miller, J. H.; Wang, K.; Snurr, R. Q. Metal Alkoxide Functionalization in Metal-Organic Frameworks for Enhanced Ambient-Temperature Hydrogen Storage. *J. Phys. Chem. C* **2011**, *115*, 2066−2075.

(66) Wu, Y.; Liu, D.; Chen, H.; Qian, Y.; Xi, H.; Xia, Q. Enhancement Effect of Lithium-Doping Functionalization on Methanol Adsorption in Copper-Based Metal-Organic Framework. *Chem. Eng. Sci.* **2015**, *123*, 1−10.

(67) Trens, P.; Belarbi, H.; Shepherd, C.; Gonzalez, P.; Ramsahye, N. A.; Lee, U. H.; Seo, Y. K.; Chang, J. S. Coadsorption of N-Hexane and Benzene Vapors onto the Chromium Terephthalate-Based Porous Material MIL-101(Cr) an Experimental and Computational Study. *J. Phys. Chem. C* **2012**, *116*, 25824−25831.

(68) Eddaoudi, M.; Kim, J.; Rosi, N.; Vodak, D.; Wachter, J.; O'Keeffe, M.; Yaghi, O. M. Systematic Design of Pore Size and Functionality in Isoreticular MOFs and Their Application in Methane Storage. *Science* **2002**, *295*, 469−472.

(69) Chui, S. S. Y.; Lo, S. M. F.; Charmant, J. P. H.; Orpen, A. G.; Williams, I. D. A Chemically Functionalizable Nanoporous Material $[Cu_3(TMA)_2(H_2o)_3]N$. *Science* **1999**, *283*, 1148−1150.

(70) Llewellyn, P. L.; Bourrelly, S.; Serre, C.; Vimont, A.; Daturi, M.; Hamon, L.; De Weireld, G.; Chang, J. S.; Hong, D. Y.; Kyu Hwang, Y.; Hwa Jhung, S.; Férey, G. High Uptakes of CO_2 and CH_4 in Mesoporous Metal—Organic Frameworks MIL-100 and MIL-101. *Langmuir* **2008**, *24*, 7245−7250.

(71) Morris, W.; He, N.; Ray, K. G.; Klonowski, P.; Furukawa, H.; Daniels, I. N.; Houndonougbo, Y. A.; Asta, M.; Yaghi, O. M.; Laird, B. B. A Combined Experimental-Computational Study on the Effect of Topology on Carbon Dioxide Adsorption in Zeolitic Imidazolate Frameworks. *J. Phys. Chem. C* **2012**, *116*, 24084−24090.

(72) Wiersum, A. D.; Soubeyrand-Lenoir, E.; Yang, Q.; Moulin, B.; Guillerm, V.; Yahia, M. B.; Bourrelly, S.; Vimont, A.; Miller, S.; Vagner, C.; Daturi, M.; Clet, G.; Serre, C.; Maurin, G.; Llewellyn, P. L. An Evaluation of UiO-66 for Gas-Based Applications. *Chem.—Asian J.* **2011**, *6*, 3270−3280.

(73) Vermoortele, F.; Vandichel, M.; Van de Voorde, B.; Ameloot, R.; Waroquier, M.; Van Speybroeck, V.; De Vos, D. E. Electronic Effects of Linker Substitution on Lewis Acid Catalysis with Metal−Organic Frameworks. *Angew. Chem., Int. Ed.* **2012**, *51*, 4887−4890.

DOI: 10.1021/am508570d
ACS Appl. Mater. Interfaces 2015, 7, 5775−5787

(74) Shearer, G. C.; Chavan, S.; Ethiraj, J.; Vitillo, J. G.; Svelle, S.; Olsbye, U.; Lamberti, C.; Bordiga, S.; Lillerud, K. P. Tuned to Perfection: Ironing out the Defects in Metal−Organic Framework UiO-66. *Chem. Mater.* **2014**, *26*, 4068−4071.
(75) Bon, V.; Senkovska, I.; Weiss, M. S.; Kaskel, S. Tailoring of Network Dimensionality and Porosity Adjustment in Zr- and Hf-Based MOFs. *CrystEngComm* **2013**, *15*, 9572−9577.
(76) Grimme, S. Semiempirical GGA-Type Density Functional Constructed with a Long-Range Dispersion Correction. *J. Comput. Chem.* **2006**, *27*, 1787−1799.
(77) Tsuzuki, S.; Honda, K.; Uchimaru, T.; Mikami, M.; Tanabe, K. Origin of Attraction and Directionality of the Π/Π Interaction: Model Chemistry Calculations of Benzene Dimer Interaction. *J. Am. Chem. Soc.* **2001**, *124*, 104−112.
(78) Hunter, C. A.; Sanders, J. K. M. The Nature of Pi-Pi Interactions. *J. Am. Chem. Soc.* **1990**, *112*, 5525−5534.
(79) Headen, T. F.; Howard, C. A.; Skipper, N. T.; Wilkinson, M. A.; Bowron, D. T.; Soper, A. K. Structure of Pi-Pi Interactions in Aromatic Liquids. *J. Am. Chem. Soc.* **2010**, *132*, 5735−5742.

DOI: 10.1021/am508570d
ACS Appl. Mater. Interfaces 2015, 7, 5775−5787